Density Functional Theory Study of Ligand Binding on CdSe (0001), (000$\bar{1}$), and (11$\bar{2}$0) Single Crystal Relaxed and Reconstructed Surfaces: Implications for Nanocrystalline Growth

Jane Y. Rempel,[†] Bernhardt L. Trout,[†] Moungi G. Bawendi,[‡] and Klavs F. Jensen*[,†]

Department of Chemical Engineering and Department of Chemistry, Massachusetts Institute of Technology, Cambridge, Massachusetts 02139

Received: June 28, 2006

To gain a better understanding of the influence of ligand−surface interactions on nanocrystalline growth, periodic density functional theory calculations were employed in the study of the binding of organic ligands on the relaxed nonpolar (11$\bar{2}$0) and polar Se terminated (000$\bar{1}$) surfaces and the relaxed and vacancy and adatom reconstructed Cd terminated (0001) surface. We examined chemisorption properties of phosphine, amine, phosphine oxide, carboxylic acid, and phosphinic acid model ligands, including preferred binding sites and geometries, vibrational frequencies, and binding energetics, and compared findings to intrinsic growth via addition of CdSe molecules or Cd and Se atoms. Our results indicate that binding of the ligands is preferred in the electron-poor 1-fold sites on all surfaces, with secondary coordination of the acidic ligands through the hydroxyl hydrogen to the electron-rich surface sites. In general ligand adsorption directly obstructs binding sites for growth species on the (11$\bar{2}$0) surface and only indirectly on the two polar surfaces. The order of binding affinities on the (11$\bar{2}$0) and (0001) surfaces is $PH_3 < OPH_3 \approx HCOOH < NH_3 < OPH_2OH$ and that on the (000$\bar{1}$) surface is $OPH_3 \approx HCOOH < OPH_2OH < NH_3 < PH_3$. Our findings corroborate the experimental observation that incorporation of the nonbulky phosphinic acid-type ligands with high affinity and high selectivity for both the (11$\bar{2}$0) and (0001) surfaces strongly enhances unidirectional growth on the (000$\bar{1}$) surface, while incorporation of either bulky ligands or ligands with moderate affinity does not. Higher affinity of all traditionally used ligands for the (11$\bar{2}$0) surface compared to the (0001) surface also suggests that new ligands should be engineered to achieve the synthesis of novel shapes that require preferential growth on the (11$\bar{2}$0) surface.

1. Introduction

Over the past decade, colloidal semiconductor nanocrystals have generated considerable interest in the scientific and industrial communities as a result of their unique size and property relationships. The importance of these nanomaterials has motivated substantial experimental research efforts spanning a broad range of composite semiconductors as summarized in several recent reviews.[1−3] Multiple applications of the nanocrystals have been explored including fluorescent labels for biological assays,[4] electroluminescent devices,[5] and lasers.[6] For many of these applications it is essential to use high-quality, monodisperse, and highly crystalline samples. As a result, many synthetic routes have been developed to achieve size and shape selective preparation routes of quality nanocrystals by using batch[7,8] or continuous-flow[9] processing.

One of the most frequently studied and well-characterized compound semiconductor nanocrystals is cadmium selenide. Nanocrystals of this material of various sizes and shapes have been successfully synthesized ranging from geometrically simple shapes such as spherical dots[7] and nanorods[10] to more exotically shaped arrows and tetrapods.[10] In the earliest preparation of high-quality CdSe quantum dots, dimethyl cadmium and tri-*n*-octylphosphine selenide (TOPSe) are rapidly injected into a hot solvent consisting of a mixture of tri-*n*-octylphospine (TOP) and tri-*n*-octylphosphine oxide (TOPO),[7] where the solvent serves a dual role as the reaction medium and as the source of surface ligands for the growing nanocrystals. Synthetic routes based on the salt precursors of cadmium, such as cadmium hydroxide[9] and cadmium oxide,[11] have also been developed. Modification of these routes by varying the relative ligand and precursor concentrations has yielded synthetic routes that can achieve tunability of the shape, size, and quality of the final nanocrystalline product.[10,12] However, much of the work in this area requires extensive trial-and-error optimization of the chemistry since the underlying crystal growth mechanisms in these systems are not yet well understood. Therefore, it is necessary to develop a general framework for studying nanocrystalline growth that would allow for rational design of new nanocrystalline materials. Moreover, since ligand selection is such an important aspect in dictating the morphology of the nanocrystals, gaining a thorough understanding of the ligand−nanocrystal interactions is vital for improved understanding of the crystal growth phenomena.

Several experimental studies have been aimed at identifying specific ligand interactions with the surfaces of the CdSe nanocrystals. For example, phosphorus nuclear magnetic resonance (^{31}P NMR)[13,14] experiments have been performed to identify the number of phosphine groups present on the surface of the nanocrystal. Band edge photoluminescence studies have been carried out to investigate the interaction of TOPO with

* Author to whom correspondence should be addressed. E-mail: kfjensen@mit.edu. Phone: (617) 253-4589. Fax: (617) 258-8224.
[†] Department of Chemical Engineering.
[‡] Department of Chemistry.

10.1021/jp064051f CCC: $33.50
Published on Web 08/23/2006

TABLE 1: Comparison of Model and Actual Ligands Utilized in the Synthesis of CdSe Nanocrystals

model	ligand	shape	precursor concn	ref
PH_3	tri-*n*-octylphosphine	spheres	low	7, 9
	tri-*n*-butylphosphine	rods	high	23
NH_3	oleylamine	spheres	low	9
OPH_3	tri-*n*-octylphosphine oxide	spheres	low	7
	tri-*n*-octylphosphine oxide	rods	high	23
HCOOH	oleic acid	spheres	low	9
OPH_2OH	hexylphosphonic acid (high concn)	rods	high	23, 10
	hexylphosphonic acid (low concn)	spheres	high	10

CdSe single-crystal surfaces.[15] A few computational studies have also been performed. Tight-binding,[16] force-field,[17] and density functional theory (DFT)[18] calculations were utilized to explore the passivation effects on small CdSe clusters. A DFT-LDA study was performed by Manna et al. investigating methylamine and methylphosphonic acid interaction effects on CdSe surfaces.[19] The goal of the present work is to utilize first principles calculations to gain a fundamental understanding of the influence organic ligands have on crystal growth on different facets of a wurtzite CdSe crystal.

Model ligands utilized in this study mimic those that are frequently employed in real experimental systems. To make the problem computationally tractable, the PH_3, NH_3, OPH_3, HCOOH, and OPH_2OH ligands have been selected as model compounds for the actual ligand species (see Table 1). Since ligands play an important role in determining the final nanocrystal shape, the morphology of the final products of the synthetic routes for each ligand are also summarized in Table 1. There are several important parameters that determine the influence of a ligand on crystal growth. Ligand *affinity* determines the strength of ligand binding to a given surface, and, therefore, how well the ligand blocks binding sites for addition of the growth species. *Specificity* determines the difference between the binding strengths on two different surfaces, thus predicting if a particular ligand binding is likely to assist in growth anisotropy. And finally *steric hindrance* determines both the packing efficiency of ligands on the surface and the ability of the ligand to sterically block binding sites for growth species adsorption. The first two parameters are directly computed in this work by using density functional theory (DFT-GGA), a method that has been utilized extensively in the past to study reactive processes on semiconductor surfaces.[20−22] The third parameter is described qualitatively by using heuristic arguments to relate the steric behavior of a model ligand to its actual counterpart.

Surfaces of the wurtzite CdSe explored in the present study include the nonpolar $(11\bar{2}0)$ surface and the two polar $(000\bar{1})$ Se terminated and (0001) Cd terminated surfaces, corresponding to the sides, top, and bottom of the nanocrystals.[24] We also explore possible reconstructions of the polar surfaces, including vacancy formation and adatom adsorption. Chemisorption behavior of the model ligands is considered in detail on both relaxed and reconstructed surfaces. In particular, we determine the preferred binding sites and binding geometries along with binding energetics of the model ligands on the relaxed and reconstructed surfaces. We also consider competitive binding of the ligands and the growth species, CdSe molecule, and Cd and Se atoms, and the ability of the ligands to block growth sites. Furthermore, we relate our findings to the experimental observation of growth anisotropy and provide insight into why some ligands are better than others at achieving particular nanocrystalline morphologies.

2. Methods

2.1. Computational Details. All first-principles calculations were performed with use of a periodic total energy density functional theory (DFT) code, DACAPO.[25] Ultrasoft pseudopotentials[26] were utilized to describe atomic core electrons, while a plane wave basis set with a kinetic energy cutoff of 25 Ry was utilized to expand the Kohn−Sham one-electron valence states. The Se pseudopotential was generated in-house with the base configuration of Se ($4s^24p^4$) for the six selenium valence electrons. The density was determined by iterative diagonalization of the Kohn−Sham Hamiltonian, Fermi population of the Kohn−Sham states ($k_BT = 0.1$ eV), and Pulay mixing of the resulting electronic density.[27] All total energies were extrapolated to $k_BT = 0$ eV. The exchange-correlation energy and potential were described self-consistently with a generalized gradient approximation, using the GGA-PW91 functional.[28,29] An $8 \times 8 \times 8$ and a $2 \times 2 \times 1$ Monkhorst−Pack[30] **k**-point sets were employed for bulk crystal and exposed surface calculations, respectively. Convergence with respect to the **k**-point set and the plane wave energy cutoff was rigorously verified, such that the total energy was converged to at most 0.1 eV and the difference in energies was converged to at most 0.01 eV. The calculated lattice parameter for a wurtzite structure of CdSe of 4.38 Å is within 1.9%[31] of the experimental value.

Surfaces of the wurtzite CdSe were described by using a slab model that contained four CdSe bilayers, each with a layer of Cd and a layer of Se atoms, and approximately 12 Å of vacuum. The nonpolar $(11\bar{2}0)$ surface (Figure 1a) was modeled with an irreducible unit cell that contained 4 Cd and 4 Se atoms per bilayer. Since each unit cell contained two, not related by symmetry, but chemically equivalent, binding sites, introduction of one ligand corresponded to 0.5 ML surface coverage. Decreasing the surface coverage by a factor of 2, in a test case of the NH_3 model ligand, led to a change of the binding energy of −0.04 eV (less than 5%), which is sufficiently small to ensure that neighboring ligands are minimally interactive. The polar Se terminated $(000\bar{1})$ and Cd terminated (0001) surfaces (Figure 1b−d) were modeled by a 2×2 lateral supercell that also contained 4 Cd and 4 Se atoms per bilayer. In this geometry, introduction of one ligand per supercell was equivalent to a 0.25 ML surface coverage that would minimize lateral ligand interactions. Reconstruction of the polar surfaces via vacancy formation or adatom adsorption was modeled either by removing one of four surface atoms or by addition of one atom of opposite type per 2×2 supercell (Figure 1e,f). In all cases the top two surface bilayers were allowed to relax while the bottom two bilayers were fixed in the bulk truncated geometry. Ligand adsorption was only allowed on one of the two exposed surfaces, while the electrostatic potential was adjusted[32] in order to decouple dipole interactions of the neighboring slabs. To verify that the neighboring slabs were sufficiently isolated, first, vacuum thickness was increased by one unit vector leading to a total energy change of less than 0.01 eV; and second, the number of bilayers was increased to either five or six, with variation in the surface energy not exceeding 2%.

2.2. Thermodynamics. For all of the unreconstructed surfaces, the surface energy of a relaxed surface was determined by using a simple slab method:

$$\sigma_{\text{top,relaxed}} = (E_{\text{slab,relaxed}} - n_{\text{CdSe}}E_{\text{bulk}})/A - \sigma_{\text{bottom}} \quad (1)$$

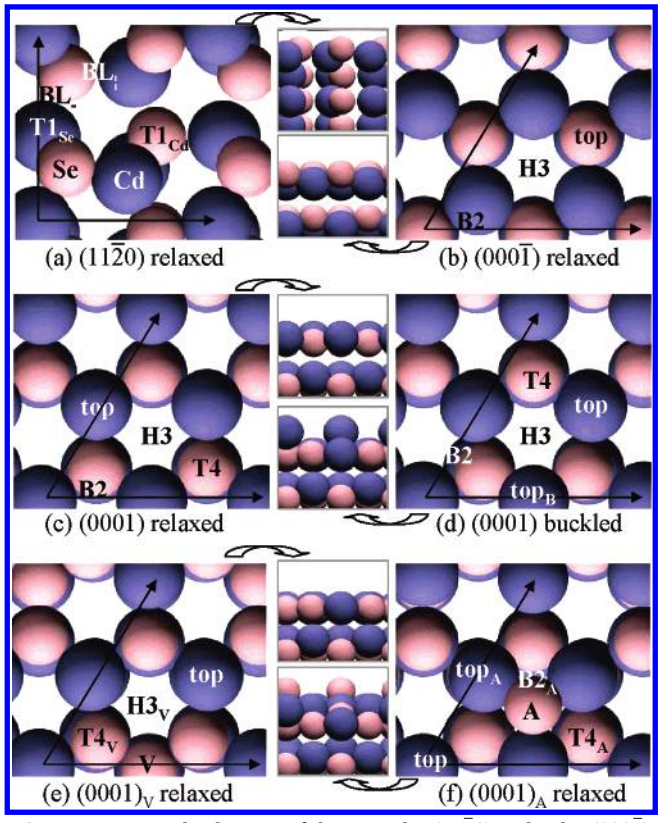

Figure 1. Top and side view of the nonpolar (11$\bar{2}$0) and polar (000$\bar{1}$) and (0001) CdSe surfaces and the vacancy and adatom surface reconstructions of the 2 × 2 supercell of the polar (0001) CdSe surface. Unit cell vectors are labeled along with the sites for adspecies and ligand adsorption. The top two surface bilayers, containing two Cd (larger spheres) and two Se (smaller spheres) layers, are relaxed.

where $E_{slab,relaxed}$ is the total energy of the slab with the top two bilayers relaxed, n_{CdSe} is the number of CdSe units in the slab, and A is the area of the supercell. The surface energy of the bottom surface for the nonpolar (11$\bar{2}$0) surface, which has identical termination on both sides of the slab ($\sigma_{top} = \sigma_{bottom}$), was calculated by using a slab without surface relaxation. In the case of the polar surfaces, where the top and bottom surfaces cannot be isolated independently in a slab geometry, we utilized a modified infinite wedge method that has been described in detail earlier.[33] It is important to note that the surface energy of the polar surfaces depends on the relative chemical potentials of the Cd and Se particle reservoirs. Assuming that the particle reservoirs are in thermal equilibrium with the bulk CdSe and there is no flow of particles from the bulk CdSe to either one of the reservoirs, two limiting values can be placed on the chemical potential of cadmium:[33]

$$E_{bulk,Cd} + \Delta H_{f,CdSe} < \mu_{Cd} < E_{bulk,Cd} \quad (2)$$

The lower limit corresponds to the Cd-poor and the upper limit to the Cd-rich regime. The enthalpy of formation is defined as:

$$\Delta H_{f,CdSe} = E_{bulk} - E_{bulk,Cd} - E_{bulk,Se} \quad (3)$$

We calculated the heat of formation to be −1.43 eV, which is in close agreement with DFT-LDA results.[19] The limits on the chemical potential of selenium can be determined from that of cadmium, since, in thermal equilibrium, the sum of the two is equal to the energy of the bulk CdSe.

Gas-phase energies of the Cd and Se atoms were used as reference states in calculating the energies of reconstruction, such that the energy of vacancy reconstruction was defined as:

$$\Delta E_{rec} = E_{slab,reconstructed} - E_{slab,relaxed} + E_{Cd\ or\ Se\ gas\ phase} \quad (4)$$

Similarly, the energy of adatom reconstruction was defined as:

$$\Delta E_{rec} = E_{slab,reconstructed} - E_{slab,relaxed} - E_{Cd\ or\ Se\ gas\ phase} \quad (5)$$

In general, the binding energy for any adsorbate (A) was defined as:

$$BE = E_{slab+A} - E_{slab,relaxed} - E_{A,gas} \quad (6)$$

where E_{slab+A} is the energy of the slab and the adsorbate and $E_{A,gas}$ is the energy of the adsorbate in the reference vacuum state. Frequencies of the ligand normal modes of vibration were determined from eigen values of the mass weighted Hessian matrix, obtained by displacing adsorbate atoms by 0.01 Å and calculating force derivates by using second-order finite difference method. The binding energies of ligands were then corrected by the zero-point energies (ZPE):

$$ZPE_c = ZPE_{slab+A} - ZPE_{A,gas} - ZPE_{slab} \quad (7)$$

ZPE_{slab} was calculated only for surfaces with one of the surface atoms protruding out of the surface plane, such that the protruding atom was moved, while the remaining slab atoms were fixed in their relaxed positions. Including motion of the protruding atom resulted in emergence of a new mode with only small changes in the frequencies of other adsorbate modes, leading to a change in ZPE correction not exceeding 0.005 eV.

3. Results and Discussion

Images of the top and side views of the nonpolar (11$\bar{2}$0) and the polar Se terminated (000$\bar{1}$) and Cd terminated (0001) surfaces are presented in Figure 1a−d. In all cases the top two surface bilayers are relaxed to an energy minimum. Images of the two stable relaxations, surface contraction and surface buckling, of the Cd terminated (0001) facet are included. Since detailed descriptions of the surface relaxation and reconstruction have been described previously,[33] we only include values for the properties that are key in describing nanocrystalline growth of CdSe. In particular, Table 2 contains the surface energy ranges, between the Cd-poor and Cd-rich limits, and also the energies for the vacancy and adatom reconstructions of the polar facets. In general, based on the surface energies the equilibrium shape of the nanoparticle can be estimated by minimizing energy at constant volume. For a hexagonal barrel the aspect ratio is equal to:

$$\frac{\sqrt{3}}{4}\frac{\sigma_{(000\bar{1})} + \sigma_{(0001)}}{\sigma_{(11\bar{2}0)}} \quad (8)$$

Comparison of the surface energies in Table 2 reveals that the nonpolar (11$\bar{2}$0) surface is thermodynamically more stable than the polar counterparts in the entire range of the Cd chemical potentials, and, as a result, we would expect this surface to grow

TABLE 2: Surface Properties of the Polar and Nonpolar CdSe Surfaces

	(11$\bar{2}$0)	(000$\bar{1}$)	(0001)
σ (meV/Å^2), Cd poor	15.4	30.9	55.8,[a] 49.7[b]
σ (meV/Å^2), Cd rich		52.4	34.3,[a] 28.2[b]
$\Delta E_{rec,V}$ (eV)		2.5	0.3
$\Delta E_{rec,A}$ (eV)		−2.1	−3.6

[a] Relaxed surface. [b] Buckled surface.

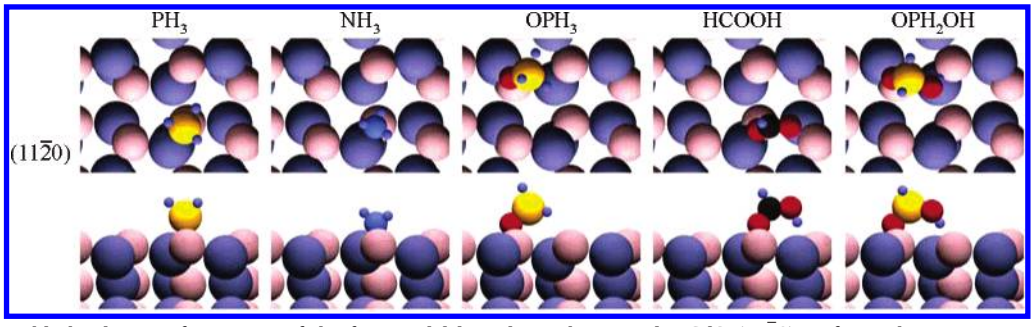

Figure 2. Most stable binding configurations of the five model ligands on the nonpolar CdSe(11$\bar{2}$0) surface. The top two surface bilayers are relaxed.

TABLE 3: Vibrational Frequencies, Binding Energy, and Distances of the Adspecies and the Five Model Ligands in the Most Stable Sites on the Nonpolar (11$\bar{2}$0) CdSe Surface[a]

	species	site	frequency[b] (cm^{-1})	BE (eV) [BE + ZPE_c]	*d* (Å)
vacuum	CdSe		192		
	PH_3		2341, 2340, 2328, 1095, 1093, 978		
	NH_3		3598, 3592, 3455, 1607, 1604, 973, 120		
	OPH_3		2334, 2323, 2320, 1217, 1100, 1077, 1074, 802, 802, 797, 110		
	HCOOH		3713, 3024, 1816, 1333, 1249, 1082, 990, 675, 675, 590, 102		
	OPH_2OH		3835, 2375, 2335, 1243, 1117, 1039, 958, 852, 852, 825, 741, 390, 227		
(11$\bar{2}$0)	Se[33]	$BL_{\|\|}$	185, 162	−2.07 [−2.05]	2.63, 2.40[c]
	Cd[33]	$BL_{\perp}$		−0.30 [−0.30]	2.91, 3.13[c]
	CdSe[33]	$T1_{Se}$-$T1_{Cd}$	265, 147, 115	−2.66 [−2.64]	2.52, 2.59
	PH_3	$T1_{Cd}$	2389, 2379, 2359, 1082, 1067, 939, 234, 230, 230, 111	−0.32 [−0.29]	2.83
	NH_3	$T1_{Cd}$	3579, 3552, 3427, 1589, 1576, 1096, 497, 460, 460, 247	−0.72 [−0.66]	2.39
	OPH_3	$T1_{Cd}$	2403, 2386, 2287, 1156, 1078, 1030, 936, 785, 785, 762, 174, 101	−0.51 [−0.51]	2.37
	HCOOH	[$T1_{Cd}$-$T1_{Se}$]	3042, 3006, 1744, 1356, 1313, 1175, 1007, 840, 840, 624, 176, 148	−0.53 [−0.54]	2.40, 3.23, 2.22
	OPH_2OH	[$T1_{Cd}$-$T1_{Se}$]	2895, 2401, 2345, 1183, 1108, 1098, 1016, 914, 914, 876, 753, 693, 386, 188, 168, 102	−0.81 [−0.80]	2.33, 3.16, 2.14

[a] Binding energy is corrected for the ZPE, shown in brackets. Distance, *d*, is defined as the bond length from the main adsorbate atom to the nearest surface atom. For acidic species, distance to the hydroxyl oxygen and hydrogen are also included in that order. Vibrational frequencies of the CdSe molecule and the five ligands in a vacuum are also presented. [b] Only frequencies above 100 cm^{-1} are included. [c] Distance to the surface Se atom.

at a slower rate. When comparing the two polar surfaces, the Se terminated (000$\bar{1}$) surface is more stable under Cd-poor conditions, while the Cd terminated (0001) surface is more stable under Cd-rich conditions. Comparison of the vacancy formation and adatom reconstruction energies, as defined in eqs 4 and 5, between the two polar surfaces (Table 2) reveals that the former is an endothermic process with lower energy cost on the (0001) surface and the later is an exothermic process with higher energy gain also on the (0001) surface. As a result, in all subsequent ligand binding calculations we chose to include only the stable reconstructions of the (0001) surface, images of which can be found in Figure 1e,f.

The following sections contain a description of the chemisorption properties of the model phosphine, amine, phosphine oxide, and carboxylic and phosphinic acid ligands (Table 1) on the nonpolar (11$\bar{2}$0) surface, the polar Se terminated (000$\bar{1}$) and Cd terminated (0001) surfaces, and the vacancy and adatom reconstructed (0001) surface. In particular, binding energetics, binding geometries, and surface relaxations are described. Binding energies are corrected for the zero point vibrational energy. The thermochemistry of ligand adsorption is then compared among ligands and across surfaces and related to the experimental observation of growth anisotropy. Furthermore, influence of ligand binding on homoepitaxy is examined by comparing energetics of ligand binding to the thermochemistry of binding and dissociation of the CdSe molecule on the relaxed and reconstructed surfaces of interest. Note that a detailed description of the atomic and molecular adsorption is covered in a separate publication.[33]

3.1. Nonpolar (11$\bar{2}$0) Surface. Several possible binding states of the five model ligands on the relaxed nonpolar (11$\bar{2}$0) surface were considered; however, only the most energetically stable configurations were explored in detail. Schematics of the five ligands in the lowest energy binding sites are presented in Figure 2, with the corresponding binding energies, geometric parameters, and normal vibrational mode frequencies listed in Table 3. The binding site labels are equivalent to those in Figure 1a, where T1 is a tetrahedral 1-fold site and BL is a 2-fold bridge site. Frequencies of the normal modes of vibration for the ligands in the gas phase are also included in Table 3 along with the zero point energy corrections. To clearly relate the competitive binding of ligands to the thermochemistry of adspecies adsorption, the chemisorption properties of the CdSe molecule and the Cd and Se atoms[33] are also listed in Table 3.

All ligands considered in this study can be divided into two types: those that bind through one atomic center (monodentate) and those that bind through two (bidentate). Phosphines, amines, and phosphine oxides belong to the first group, while carboxylic

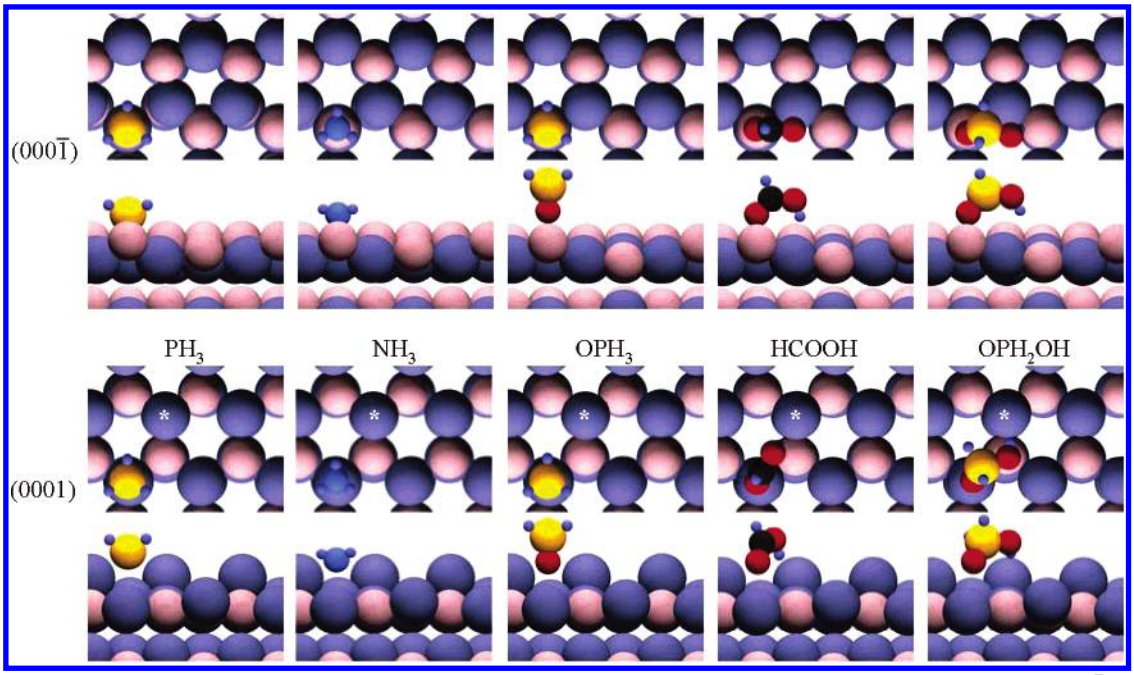

Figure 3. Most stable binding configurations of the five model ligands on the polar buckling CdSe(0001) and contracted CdSe(000$\bar{1}$) surfaces. The top two surface bilayers are relaxed. Buckling sites are labeled with an asterisk. For simplicity, periodic copies of the ligands are not shown.

and phosphinic acids belong to the second. All monodentate ligands on the nonpolar (11$\bar{2}$0) surface prefer to bind to the surface Cd atom in the T1$_{Cd}$ site, while the bidentate acidic ligands prefer to coordinate to the surface Cd atom through the oxygen atom and to the surface Se atom through the hydroxyl hydrogen in the T1$_{Cd}$-T1$_{Se}$ site (Figure 2). This is consistent with the electron-donating atomic centers (P, N, O) binding to the electron-poor Cd site, and the electron-withdrawing hydroxyl hydrogen binding to the electron-rich Se site. Comparison of the binding geometries in Figure 2 to the relaxed surface in the absence of ligands (Figure 1a) reveals that introducing a ligand alters the relaxation geometry of the surface. In particular, the geometry around the coordinating Cd atom changes from nearly planar to approximately tetrahedral, which can be observed by examining the out-of-plane tilt of the coordinating Cd to the surface Se bond. This geometry change is especially significant for NH_3, HCOOH, and OPH_2OH. Comparison of the normal mode vibrational frequencies of the ligands on the surface to the ligands in the reference state (Table 3) shows small changes for the monodentate ligands and only considerable damping of the highest frequency OH stretching mode for the bidentate acidic ligands. The change in vibrational frequencies leads to a small ZPE correction of the binding energies of up to 0.06 eV. Note that in general the ZPE correction to the binding energy is positive; however, if the decrease in the OH stretching frequency is large, the correction can be slightly negative. On the (11$\bar{2}$0) surface, the ZPE corrected binding energies vary between −0.29 and −0.80 eV with the ligands arranged from the weakest to the strongest binding: $PH_3 < OPH_3 \approx$ HCOOH $< NH_3 < OPH_2OH$. The trend in the binding energies is similar to the trend in the extent of change in the surface relaxation.

If we now consider binding preferences of the atomic and molecular adspecies, Table 3, we see that the CdSe molecule and Cd and Se atoms prefer to coordinate to both surface Cd and surface Se. In particular, the CdSe molecule prefers the T1$_{Se}$-T1$_{Cd}$ binding site, while atomic Cd and Se prefer the BL$_{\|}$ and BL$_{\perp}$ sites, respectively. Note that the T1$_{Cd}$ site is also the preferred site for the adsorption of monodentate ligands and both the T1$_{Cd}$ and T1$_{Se}$ are important for the adsorption of bidentate ligands. Therefore, we would expect ligands to competitively bind on the (11$\bar{2}$0) surface and hinder growth by blocking the binding sites for the addition of the growth species.

3.2. Polar (000$\bar{1}$) and (0001) Surfaces. Figure 3 contains schematics of the five ligands in the lowest energy binding sites on the polar Se terminated (000$\bar{1}$) and Cd terminated (0001) surfaces. Several initial ligand configurations were considered on these surfaces; however, only the most stable binding geometries were explored in detail. The corresponding binding energies, geometric parameters, and normal vibrational mode frequencies are listed in Table 4. Site labels in Table 4 are described in Figure 1b−d, where top is a 1-fold atop site, B2 is a 2-fold bridge site, H3 is a hollow 3-fold site, and T4 is a tetrahedral 4-fold site. Similar to the comparison performed on the (11$\bar{2}$0) surface, the chemisorption properties of the CdSe molecule and the Cd and Se atoms[33] are also listed in Table 4.

On the Se terminated (000$\bar{1}$) surface, both monodentate and bidentate ligands prefer to bind in the top site with the bidentate acidic ligands also coordinating the nearest surface Se atom (Figure 3). However, unlike adsorption on the (11$\bar{2}$0) surface where all ligands bind in close proximity to the coordinating Cd center and exhibit moderate to strong binding energies, on the (000$\bar{1}$) surface, only the PH_3 and the NH_3 model ligands associate strongly to the surface, with the ZPE corrected binding energy of −0.88 and −0.46 eV, respectively (Table 4). The OPH_2OH, on the other hand, is only weakly binding, with the ZPE corrected binding energy of −0.24 eV, which is primarily attributed to hydroxyl hydrogen coordination of the neighboring electron-rich surface Se atom. Consistent with weaker binding, the decrease in the frequency of the OH stretch is smaller on the (000$\bar{1}$) surface than on the (11$\bar{2}$0) surface. The OPH_3 and HCOOH ligands are effectively nonbinding, and as a result we did not calculate ZPE corrections for these species. Comparison of the binding geometries in Figure 3 to the ligand free surface in Figure 1b reveals that surface relaxation is altered as a result of ligand binding. In the case of the strongly binding ligands, the noncoordinating Se atoms move above the surface plane, while the nearest subsurface Cd atoms move radially outward from the coordinating center. Conversely, introduction of the

TABLE 4: Vibrational Frequencies, Binding Energy, and Distances of the Adspecies and the Five Model Ligands in the Most Stable Sites on the Polar (000$\bar{1}$) and (0001) CdSe Surfaces[a]

	species	site	frequency[b] (cm^{-1})	BE (eV) [BE + ZPE_c]	d (Å)
(000$\bar{1}$)	Se[33]	B2	186, 134	−2.90 [−2.88]	2.44
	Cd[33]	H3	105, 105	−2.09 [−2.08]	2.76
	CdSe[33]	[H3-B2]	246, 106	−2.63 [−2.62]	2.53, 3.32
	PH_3	top	2407, 2405, 2384, 1036, 1033, 960, 593, 592, 592, 338	−0.98 [−0.88]	2.16
	NH_3	top	3567, 3510, 3363, 1560, 1533, 1003, 659, 324, 324, 117	−0.50 [−0.46]	2.18
	OPH_3	top	-	0.03 [−]	2.97
	HCOOH	top-top	-	−0.03 [−]	2.77, 3.39, 2.47
	OPH_2OH	top-top	3290, 2385, 2347, 1172, 1103, 1022, 995, 875, 875, 862, 745, 557, 383, 132, 107	−0.24 [−0.24]	2.83, 3.30, 2.32
(0001)	Se[33]	H3	152, 105, 105	−3.59 [−3.57]	2.76
	Cd[33]	top_B	-	−0.35 [−0.35]	2.96
	CdSe[33]	[T4-B2]	184, 149	−3.27 [−3.26]	2.74, 2.73
	PH_3	top	2371, 2371, 2350, 1087, 1084, 953, 268, 239, 239, 154, 104	−0.25 [−0.20]	2.89
	NH_3	top	3576, 3561, 3428, 1594, 1582, 1091, 492, 462, 462, 200	−0.58 [−0.52]	2.42
	OPH_3	top	2349, 2348, 2344, 1198, 1096, 1073, 1058, 800, 800, 795	−0.31 [−0.32]	2.42
	HCOOH	top-top_B	3148, 3016, 1742, 1354, 1278, 1103, 1014, 737, 737, 614, 236, 164, 124, 104	−0.39 [−0.40]	2.46, 3.41, 2.40
	OPH_2OH	top-top_B	2964, 2412, 2368, 1110, 1065, 1043, 984, 886, 886, 867, 722, 546, 378, 134, 108	−0.62 [−0.64]	2.35, 3.55, 3.03

[a] Binding energy is corrected for the ZPE, shown in brackets. Distance definition follows that in Table 3. [b] Only frequencies above 100 cm^{-1} are included.

weakly or nonbinding ligands leads to a depression of the coordinating Se. The almost coplanar geometry of the Se with the subsurface Cd layer in this case suggests that electrons are transferred from the coordinating to the three noncoordinating Se atoms in a 2×2 supercell, thus leading to a change in the coordinating Se orbital hybridization from sp^3 to sp^2, making the coordinating site electron poor.

Ligand binding on the Cd terminated (0001) surface also preferentially occurs on a 1-fold top site for the monodentate and in the top-top_B site for the bidentate ligands (Figure 3). Similar to the trend on the (11$\bar{2}$0) surface, the electron-donating ligand centers (P, N, O) prefer to bind to the slightly electron-poor Cd atop site, while the electron-withdrawing hydroxyl hydrogen prefers to bind to the electron-rich buckling Cd site. The change in surface relaxation is also similar to that observed on the (11$\bar{2}$0) surface. Comparison of the surface geometries in the presence and absence of ligands, Figure 3 and Figure 1d, respectively, reveals that in the presence of ligands, the coordinating surface Cd atom moves from below the surface plane toward the surface assuming a more tetrahedral geometry. The ZPE corrected binding energies on the (0001) surface vary between −0.20 and −0.64 eV with the ligands arranged from the weakest to the strongest binding: PH_3 < OPH_3 < HCOOH < NH_3 < OPH_2OH. The order of binding strengths is similar to that on the (11$\bar{2}$0) surface. However, since the electron transfer from the three surface Cd atoms to the buckling Cd on the (0001) surface is less effective than the electron transfer from the surface Cd to the surface Se atoms on the (11$\bar{2}$0) surface, the ligand binding is consistently weaker on the (0001) than on the (11$\bar{2}$0) surface. Such that the binding strength is 0.1−0.2 eV lower, the bond lengths from the main adsorbate atom to the coordinating Cd atom is 0.02−0.06 Å longer, and the decrease in the hydroxyl stretch frequency for the bidentate species is also slightly lower (Table 4).

Comparison of the binding preferences of the Cd and Se atoms and CdSe molecule in Table 4 reveals that in general adspecies prefer to occupy multifold sites, with an exception of the Cd atom that prefers to bind atop the buckling surface Cd on the (0001) surface. In particular, CdSe prefers to bind in the T4-B2 site on both polar surfaces, while Cd and Se atoms prefer the H3 and B2 sites, respectively, on the (000$\bar{1}$) surface, and Se prefers the H3 site on the (0001) surface. In all cases, the preferred atop site for monodentate ligand binding does not directly obstruct binding of the adspecies, while the preferred top-top or top-top_B site for the bidentate ligands can potentially obstruct the B2, H3, and T4 sites. However, since bidentate ligand binding on the (000$\bar{1}$) surface is weak, adspecies adsorption on the Cd terminated (0001) surface is more likely to be influenced by the competitive ligand binding than on the (000$\bar{1}$) surface. Nonetheless, a more detailed study on the coadsorption behavior of ligands and adspecies would be necessary to determine to what extent ligand binding hinders adspecies adsorption on the polar surfaces.

3.3. Reconstructed $(0001)_V$ and $(0001)_A$ Surfaces. Based on the observation that ligand binding is preferred in the electron-poor top site on the buckling (0001) Cd terminated surface, only binding in the top site furthest from the electron-rich reconstruction center was considered on both the vacancy and adatom reconstructed surfaces. Schematic representations of the five model ligands on these surfaces are presented in Figure 4. The associated geometric parameters, binding energies, and normal mode vibrational frequencies are presented in Table 5. Site labels in Table 5 correspond to those in Figure 1e,f, with the notation similar to that on the polar unreconstructed surface, with sites adjacent to the vacancy or the adatom labeled V and A, respectively. For comparison, chemisorption properties of the adspecies, CdSe molecule, and the Cd and Se atoms[33] are also included in Table 5.

Comparison of the ligand binding energies on the reconstructed and buckling (0001) surface, Table 5 and Table 4, respectively, indicates that introduction of a vacancy in general decreases the strength of ligand binding, while introduction of a Se adatom increases the strength of ligand binding. This is not surprising, since electron transfer from the coordinating Cd

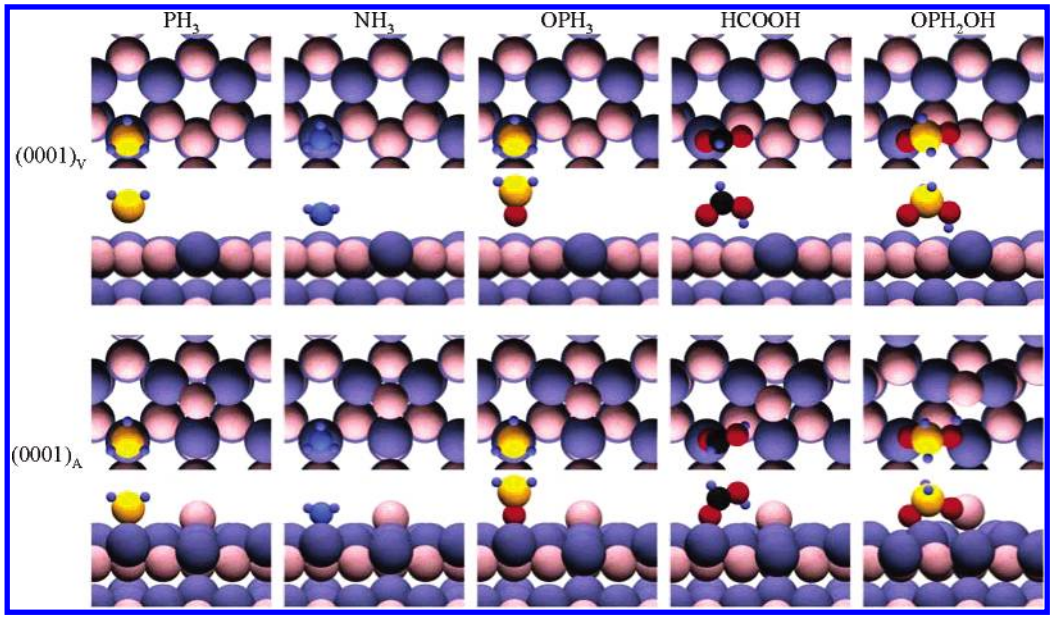

Figure 4. Most stable binding configurations of the five model ligands on the vacancy and adatom reconstructions of the CdSe(0001) surface. The top two surface bilayers are relaxed. For simplicity, periodic copies of the ligands and the Se adatom are not shown.

TABLE 5: Vibrational Frequencies, Binding Energies, and Geometric Parameters of the Adspecies and Five Ligands in the Most Stable Sites on the Reconstructed $(0001)_V$ and $(0001)_A$ CdSe Surfaces[a]

	species	site	frequency[b] (cm^{-1})	BE (eV) [BE + ZPE_c]	*d* (Å)
$(0001)_V$	Se^{33}	$T4_V$	215	−1.42 [−1.41]	2.34
	Cd^{33}	V	-	−0.33 [−0.33]	2.96
	$CdSe^{33}$	[V-$H3_V$]	171, 119, 110	−2.85 [−2.84]	2.56, 2.76
	PH_3	top	2370, 2365, 2346, 1090, 1085, 964, 215, 213, 213, 114, 111, 107	−0.19 [−0.14]	2.98
	NH_3	top	3588, 3588, 3446, 1593, 1592, 1059, 435, 418, 418, 217, 106	−0.47 [−0.41]	2.48
	OPH_3	top	2341, 2333, 2331, 1222, 1100, 1075, 1075, 796, 796, 793, 110, 107, 101	−0.17 [−0.16]	2.52
	HCOOH	top-V	3190, 3030, 1739, 1344, 1284, 1160, 1006, 792, 792, 635, 211, 179	−0.46 [−0.47]	2.51, 3.97, 3.44
	OPH_2OH	top-V	3090, 2369, 2345, 1182, 1121, 1073, 999, 899, 899, 857, 758, 550, 397, 194, 132	−0.59 [−0.59]	2.40, 3.21, 2.22
$(0001)_A$	clean		151, 104, 104		
	Se^{33}	top_A	265, 149, 125	−3.07 [−3.06]	2.62, 2.79[c]
	Cd^{33}	$T4_A$	184	−0.75 [−0.75]	2.74, 2.73[c]
	$CdSe^{33}$	[$T4_A$-top]	274, 188, 155, 145	−3.40 [−3.39]	3.35, 2.77, 2.59[c]
	PH_3	top	2396, 2389, 2369, 1086, 1085, 958, 307, 285, 285, 165, 158, 101	−0.34 [−0.29]	2.98
	NH_3	top	3569, 3567, 3441, 1593, 1593, 1138, 494, 489, 489, 221, 160	−0.66 [−0.60]	2.41
	OPH_3	top	2361, 2361, 2359, 1195, 1100, 1066, 1066, 798, 798, 797, 147	−0.45 [−0.46]	2.40
	HCOOH	top-A	3261, 3028, 1699, 1350, 1198, 1097, 993, 769, 769, 600, 192, 176, 165, 144, 105	−0.52 [−0.53]	2.43, 3.42, 2.48
	OPH_2OH	top-A	2406, 2373, 2234, 1161, 1143, 1088, 1005, 913, 913, 898, 771, 742, 398, 216, 204, 168, 118, 109	−0.99 [−1.01]	2.29, 3.12, 2.06

[a] Binding energy is corrected for the ZPE, shown in brackets. Distance definition follows that in Table 3. [b] Only frequencies above 100 cm^{-1} are included. [c] Distance to the surface Se adatom.

to either the vacancy site or the Se adatom is more effective in the later case, therefore making the Cd site more reactive for ligand binding on the $(0001)_A$ surface. One exception to this observation is HCOOH binding on the vacancy reconstructed surface, which changes the order of ligand binding strengths to $PH_3 \approx OPH_3 < NH_3 \approx HCOOH < OPH_2OH$. Note that the order remains the same on the $(0001)_A$ surface as on the unreconstructed counterpart: $PH_3 < OPH_3 < HCOOH < NH_3 < OPH_2OH$. The corresponding ZPE corrected binding energies vary between −0.14 and −0.59 eV on the $(0001)_V$ surface and between −0.29 and −1.01 eV on the $(0001)_A$ surface (Table 5). Further comparison of the binding energies indicates that binding strength of OPH_2OH on the adatom reconstructed surface is increased to a higher degree than of any other ligand. This can be attributed to a strong interaction of the hydroxyl H with the surface Se, exhibited by a much lower OH stretch frequency and by a shift of the surface Se from the 3-fold hcp site to a neighboring 2-fold site. Comparison of the surface geometries in the presence and absence of ligands, Figure 4 and Figure 1e,f, respectively, indicated that on both the vacancy and the adatom reconstructed surfaces the coordinating Cd atom, which is almost coplanar with the subsurface Se layer in the

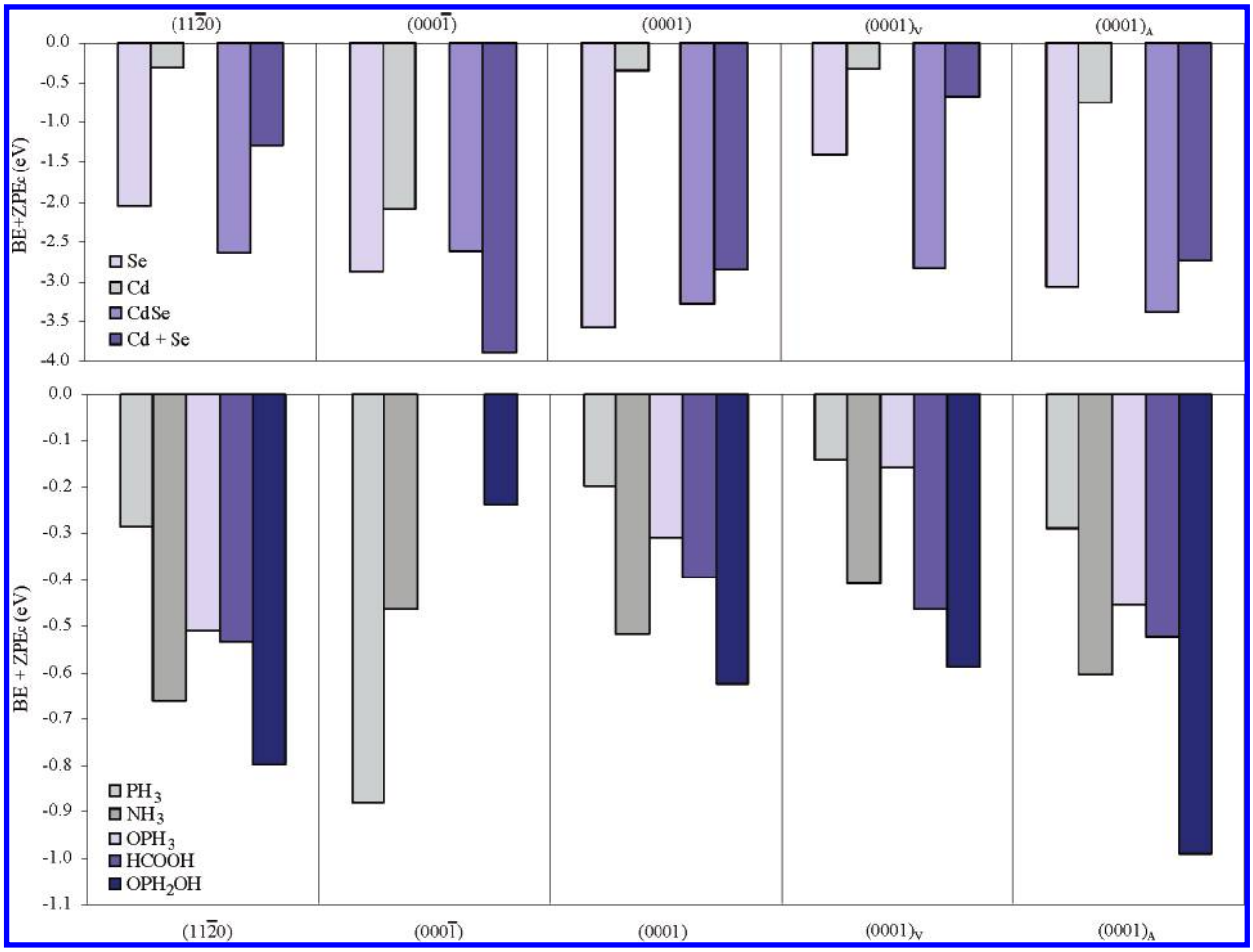

Figure 5. Schematic comparing the ZPE corrected binding energies of the adspecies and the five ligands on the three relaxed and two reconstructed surfaces. Notice that the energy scale is different for the adspecies and the ligands.

absence of ligands, moves closer to the surface plane achieving a more tetrahedral geometry. A similar effect is observed on the unreconstructed surface.

Reconstruction of the (0001) surface via vacancy and adatom formation changes site preferences for the adsorption of the adspecies, such that both the CdSe molecule and the Cd and Se atoms prefer to bind in the vicinity of the reconstruction site (Table 5). In particular, the V-H3$_V$, V, and T4$_V$ sites respectively are favored on the (0001)$_V$ surface; and the T4$_A$-top, T4$_A$, and top$_A$ sites respectively are favored on the (0001)$_A$ surface. Therefore, binding of the monodentate ligands in the top site does not block adsorption of the adspecies, with an exception of the CdSe on the adatom reconstructed surface. However, binding of the bidentate ligands in the top-V or the top-A sites can partially block the binding sites of the adspecies.

3.4. Comparative Ligand Binding and Homoepitaxy. When considering the effect of ligands on crystal growth, we first have to address variations in homoepitaxy thermodynamics on different surfaces. Therefore, chemisorption energetics for the adsorption of Cd and Se atoms and adsorption and dissociation of the CdSe molecule are summarized in Figure 5. It is important to point out that the binding energy of adspecies is presented relative to $CdSe_g$ or Cd_g and Se_g. In an actual synthetic system the coordination of the CdSe molecule in solution will decrease the energy of the reference state and, as a result, the absolute binding energy of the species making it comparable to binding energy of ligands. Comparison of the adspecies adsorption thermochemistry in Figure 5 reveals that the CdSe molecule is thermodynamically more likely to adsorb and dissociate on the Se terminated (000$\bar{1}$) surface than to adsorb on the Cd terminated (0001) facet or the (11$\bar{2}$0) facet, with an energy difference between the two processes of −0.63 and −1.25 eV, respectively. Furthermore, as discussed in sections 3.1−3.3, blocking of the binding sites by ligands is particularly important on the (11$\bar{2}$0) and (0001) surfaces, while blocking of the binding sites on the (000$\bar{1}$) by the stronger binding monodentate ligands is not as effective. Therefore, under reaction controlled regime, where growth by adspecies addition on the (000$\bar{1}$) facet is thermodynamically favored, addition of ligands that are able to block reaction sites for adspecies adsorption and also have high affinity and specificity either for the (11$\bar{2}$0) surface or both the (11$\bar{2}$0) and the (0001) surface would further enhance the preferential growth along the *c*-axis of the nanocrystals, leading to formation of nanocrystals with a high aspect ratio. On the other hand, utilization of ligands with low affinity or low selectivity would aid in uniform growth on all surfaces.

Chemisorption energetics of the PH_3, NH_3, OPH_3, HCOOH, and OPH_2OH ligands on the relaxed (11$\bar{2}$0) and (000$\bar{1}$) surfaces and the relaxed and reconstructed (0001) surface are also summarized in Figure 5. Note that values for the ZPE corrected binding energy are not included for the phosphine oxide and the carboxylic acid on the (000$\bar{1}$) surface, since both ligands are effectively nonbinding. In general, all considered ligands, with the exception of the phosphine, which prefers to bind on the Se terminated (000$\bar{1}$) surface by 0.6−0.7 eV, prefer the nonpolar (11$\bar{2}$0) surface. The difference in affinity between the (11$\bar{2}$0) and (0001) surfaces is small, only 0.1−0.2 eV, in comparison to the difference between the (11$\bar{2}$0) and (000$\bar{1}$)

surfaces, about 0.5 eV for the oxide and acids. The NH_3 ligand is an exception, with approximately equal affinity for the (0001) and (000$\bar{1}$) surfaces. Moreover, if the (0001) surface is present in the reconstructed form the driving force for binding on this surface is decreased in the case of vacancy reconstruction and increased in the case of the adatom reconstruction.

When comparing variations in the binding strengths, it is also important to consider steric effects. For example, in a real growth solution trialkylphosphine and trialkylphosphine oxides are typically utilized, and as a result the PH_3 and OPH_3 represent fairly bulky ligands, which due to crowding effects are likely to adsorb at low coverages. Consequently, even though PH_3 is very strongly bound on the (000$\bar{1}$) surface and OPH_3 is strongly bound on the (11$\bar{2}$0) surface and moderately on the (0001) surface, we would expect that many sites would still be available for adspecies addition on all of these surfaces, and, as a result, these ligands would not promote significant growth anisotropy. On the other hand, NH_3, HCOOH, and OPH_2OH represent less sterically hindered monoalkyl ligands, which we would expect to pack closer on the surface. Hence, for these species relative binding strengths on different facets become important when considering growth anisotropy. Specifically, all three ligands have higher affinity for the nonpolar (11$\bar{2}$0) surface that corresponds to the sides of the rod-shaped nanocrystals; therefore, both amines and acids would likely hinder adspecies addition on the (11$\bar{2}$0) surface leading to preferential growth along the *c*-axis of the wurtzite crystal. When differentiating between (0001) and (000$\bar{1}$) polar surfaces, HCOOH and OPH_2-OH have higher affinity for the (0001) surface, while NH_3 binds equally strongly to both; as a result, acidic species are more likely to promote the growth on the Se terminated (000$\bar{1}$) surface while amines are not likely to differentiate between the two surfaces. Moreover, out of these three ligands, OPH_2OH is the stronger binding one with highest specificity for the (11$\bar{2}$0) over the (000$\bar{1}$) surface (Figure 5); therefore, we would expect OPH_2-OH-type ligands to be more effective in promoting growth anisotropy than the NH_3 and HCOOH type. It is also worth pointing out that if we compare binding strengths of the monodentate OPH_3 to those of the bidentate OPH_2OH on both the (11$\bar{2}$0) and the (0001) surfaces (Figure 5) we observe an increase in the binding strengths of about 0.3 eV. Therefore, we would expect that introducing a second hydroxyl group, in the form of a phosphonic acid, would lead to a ligand with higher affinity and specificity for these surfaces, which would be even better than OPH_2OH at promoting unidirectional growth.

4. Conclusions

To gain insight into the influence ligand−surface interactions have on nanocrystalline growth, we explored binding of several model species on the nonpolar (11$\bar{2}$0) surface, polar Se terminated (000$\bar{1}$) surface, and Cd terminated (0001) relaxed and reconstructed surfaces of the wurtzite CdSe crystal using periodic density functional theory (DFT-GGA) calculations. In particular, we explored binding of the PH_3, NH_3, OPH_3, HCOOH, and OPH_2OH species that mimic ligands that are traditionally employed in the synthesis of CdSe semiconductor nanocrystals. For all of these species, we determined the preferred binding geometries, vibrational frequencies, and binding energetics on the three surfaces of interest. We also related preferred binding sites for ligand binding to the preferred sites for adspecies adsorption. Furthermore, we linked these finding to the observed directional growth in some CdSe nanocrystals systems.

Out of all considered ligands, only PH_3 preferentially binds on the Se terminated (000$\bar{1}$) surface with the ligands binding in the following order: $OPH_3 \approx HCOOH < OPH_2OH < NH_3 < PH_3$. On the other hand, all other ligands favor the relaxed (11$\bar{2}$0) nonpolar surface, with the order of binding $PH_3 < OPH_3 \approx HCOOH < NH_3 < OPH_2OH$. Binding strengths on the polar (0001) Cd terminated surface follow the same trend. We find that the model PH_3 ligand has high affinity and high selectivity for the (000$\bar{1}$) facet, NH_3 has high affinity but low selectivity for the (11$\bar{2}$0) surface, OPH_3 and HCOOH have intermediate affinity but high selectivity for the (11$\bar{2}$0) surface, and OPH_2-OH has high affinity and high selectivity for the (11$\bar{2}$0) facet.

On the basis of the strong affinity and high selectivity, we would expect OPH_2OH-type ligands to be more effective in promoting anisotropic growth on the Se terminated polar facet under reaction controlled regime by competitively adsorbing and selectively blocking growth sites on the (11$\bar{2}$0) and (0001) surfaces. This phenomenon has been noted experimentally with the frequent use of phosphonic acids in the synthesis of nanorods. In contrast, the bulky trialkylphosphine ligands (modeled with PH_3) are more likely to adsorb at low coverages, and, as a result, even though they have high affinity and high selectivity for the Se terminated polar (000$\bar{1}$) surface, we would not expect these ligand to strongly influence growth anisotropy. This finding explains the experimental use of tryalkylphosphines in the synthesis of quantum dots. Similarly ligands with moderate affinities, such as phopshine oxides and carboxylic acids, have also been utilized in the synthesis of quantum dots.

Furthermore, the use of amine species that have a high affinity but a low selectivity between the two polar surfaces might be important when growth on both the (0001) and (000$\bar{1}$) facets is required. For example, in the synthesis of composite dumbbell shaped nanocrystals that requires growth on both top and bottom but not the sides of the rod-shaped nanocrystal seed, amines would play an important role in allowing the growth to proceed in both directions. Our results also suggest that all traditionally used ligand types in the synthesis of CdSe nanocrystals have a slightly higher affinity for the nonpolar side surface than for the polar Cd terminated (0001) surface, independent of affinity for the Se terminated facet. As a result, if the desired shape of the nanocrystal requires preferential growth on the (11$\bar{2}$0) facet, for example disk-shaped nanocrystals, new ligands must be developed that are drastically different from the accepted ligand types that are presently in use.

Acknowledgment. Financial support was provided in part by the NSF-MRSEC program (DMR 0213282), by the U.S. Army through the Institute for Soldier Nanotechnologies, under Contract DAAD-19-02-0002 with the U.S. Army Research Office, and by the Hertz Foundation graduate fellowship to J.R. The authors would like to acknowledge computational resources provided by the National Center for Supercomputing Applications (NCSA), the San Diego Supercomputer Center (SDSC), and the Boston University Scientific Computing Facilities.

References and Notes

(1) Alivisatos, A. P. Perspectives on the Physical Chemistry of Semiconductor Nanocrystals. *J. Phys. Chem.* **1996**, *100*, 13226−13239.

(2) Murray, C. B.; Kagan, C. R.; Bawendi, M. G. Synthesis and Characterization of Monodisperse Nanocrystals and Close-Packed Nanocrystal Assemblies. *Annu. Rev. Mater. Sci.* **2000**, *30*, 545−610.

(3) Trindade, T.; O'Brien, P.; Pickett, N. L. Nanocrystalline Semiconductors: Synthesis, Properties, and Perspectives. *Chem. Mater.* **2001**, *13*, 3843−3858.

(4) Parak, W. J.; Gerion, D.; Pellegrino, T.; Zanchet, D.; Micheel, C.; Williams, S. C.; Boudreau, R.; Gros, M. A. L.; Larabell, C. A.; Alivisatos, A. P. Biological Applications of Colloidal Nanocrystals. *Nanotechnology* **2003**, *14* (7), R15−R27.

(5) Coe, S.; Woo, W. K.; Bawendi, M. G.; Bulovic, V. Electroluminescence from Single Monolayers of Nanocrystals in Molecular Organic Devices. *Nature* **2002**, *420*, 800−803.

(6) Klimov, V. I.; Mikhailovsky, A. A.; Xu, S.; Malko, A.; Hollingsworth, J. A.; Leatherdale, C. A.; Eisler, H. J.; Bawendi, M. G. Optical Gain and Stimulated Emission in Nanocrystal Quantum Dots. *Science* **2000**, *290*, 314−317.

(7) Murray, C. B.; Norris, D. J.; Bawendi, M. G. Synthesis and Characterization of Nearly Monodisperse CdE (E = S, Se, Te) Semiconductor Nanocrystallites. *J. Am. Chem. Soc.* **1993**, *115*, 8706−8715.

(8) Dabbousi, B. O.; Rodriguez-Viejo, J.; Mikulec, F. V.; Heine, J. R.; Mattoussi, H.; Ober, R.; Jensen, K. F.; Bawendi, M. G. (CdSe)ZnS Core−Shell Quantum Dots: Synthesis and Characterization of a Size Series of Highly Luminescent Nanocrystallites. *J. Phys. Chem. B* **1997**, *101*, 9463−9475.

(9) Yen, B. K. H.; Gunther, A.; Schmidt, M. A.; Jensen, K. F.; Bawendi, M. G. A Microfabricated Gas−Liquid Segmented Flow Reactor for High-Temperature Synthesis: The Case of CdSe Quantum Dots. *Angew. Chem. Int. Ed.* **2005**, *44*, 5447−5451.

(10) Manna, L.; Scher, E. C.; Alivisatos, A. P. Synthesis of Soluble and Processable Rod-, Arrow-, Teardrop-, and Tetrapod-shaped CdSe Nanocrystals. *J. Am. Chem. Soc.* **2000**, *122*, 12700−12706.

(11) Peng, Z. A.; Peng, X. Nearly Monodisperse and Shape-Controlled CdSe Nanocrystals via Alternative Routes: Nucleation and Growth. *J. Am. Chem. Soc.* **2002**, *124*, 3343−3353.

(12) Manna, L.; Scher, E. C.; Alivisatos, A. P. Shape Control of Colloidal Semiconductor Nanocrystals. *J. Cluster Sci.* **2002**, *13* (4), 521−532.

(13) Sachleben, J. R.; Colvin, V.; Emsley, L.; Wooten, E. W.; Alivisatos, A. P. Solution-state NMR Studies of the Surface Structure and Dynamics of Semiconductor Nanocrystals. *J. Phys. Chem. B* **1998**, *102* (50), 10117−10128.

(14) Becerra, L. R.; Murray, C. B.; Griffin, R. G.; Bawendi, M. G. Investigation of the Surface Morphology of Capped CdSe Nanocrystallites by ^{31}P Nuclear Magnetic Resonance. *J. Chem. Phys.* **1994**, *100* (4), 3297−3300.

(15) Lorenz, J. K.; Ellis, A. B. Surfactant-Semiconductor Interfaces: Perturbation of the Photoluminescence of Bulk Cadmium Selenide by Adsorption of Tri-*n*-octylphosphine Oxide as a Probe of Solution Aggregation with Relevance to Nanocrystal Stabilization. *J. Am. Chem. Soc.* **1998**, *120*, 10970−10975.

(16) Pokrant, S.; Whaley, K. Tight-binding studies of surface effects on electronic structure of CdSe nanocrystals: the role of organic ligands, surface reconstruction, and inorganic capping shells. *Eur. Phys. J. D* **1999**, *6* (2), 255−267.

(17) Rabani, E. Structure and electrostatic properties of passivated CdSe nanocrystals. *J. Chem. Phys.* **2001**, *115* (3), 1493−1497.

(18) Puzder, A.; Williamson, A. J.; Zaitseva, N.; Galli, G.; Manna, L.; Alivisatos, A. P. First-Principles Simulations of the Interaction between CdSe Nanoparticles and Organic Molecules: Effects on Nanoparticle Growth. *Nano Lett.* **2004**, *4* (12), 2361−2365.

(19) Manna, L.; Wang, L. W.; Cingolani, R.; Alivisatos, A. P. First-Principles Modeling of Unpassivated and Surfactant-Passivated Bulk Facets of Wurtzite CdSe: A Model System for Studying the Anisotropic Growth of CdSe Nanocrystals. *J. Phys. Chem. B* **2005**, *109* (13), 6183−6192.

(20) Zhang, L.; Tang, H. F., J.; Mavrikakis, M.; Kuech, T. F. The addition of Sb as a surfactant to GaN growth by metal organic vapor phase epitaxy. *J. Appl. Phys.* **2002**, *92* (5), 2304−2309.

(21) Liu, Z. Y.; Gokhale, A. A.; Mavrikakis, M.; Saulys, D. A.; Kuech, T. F. Modifications of the electronic structure of GaSb surface by chalcogen atoms: S, Se, and Te. *J. Appl. Phys.* **2004**, *96* (8), 4302−4307.

(22) Kratzer, P.; Hammer, B.; Nørskov, J. K. The coupling between adsorption dynamics and the surface-structure H2 on Si(100). *Chem. Phys. Lett.* **1994**, *229*, 645.

(23) Peng, X.; Manna, L.; Yang, W.; Wickham, J.; Scher, E. C.; Kadavanich, A. V.; Alivisatos, A. P. Shape Control of CdSe Nanocrystals. *Nature* **2000**, *404*, 59−61.

(24) Shiang, J. J.; Kadavanich, A. V.; Grubbs, R. K.; Alivisatos, A. P. Symmetry of Annealed Wurtzite CdSe Nanocrystals: Assignment to the C_{3v} Point Group. *J. Phys. Chem.* **1995**, *99*, 17417−17422.

(25) Hammer, B.; Hansen, L. B.; Nørskov, J. K. Improved Adsorption Energetics within Density-Functional Theory Using Revised Perdew−Burke−Ernzerhof Functionals. *Phys. Rev. B* **1999**, *59* (11), 7413−7421.

(26) Vanderbilt, D. Soft Self-consistent Pseudopotentials in a Generalized Eigenvalue Formalism. *Phys. Rev. B* **1990**, *41* (11), 7892−7895.

(27) Kresse, G.; Furthmuller, J. Efficiency of ab initio total energy calculations for metals and semiconductors using a plane-wave basis set. *Comput. Mater. Sci.* **1996**, *6* (1), 15−50.

(28) Perdew, J. P.; Chevary, J. A.; Vosko, S. H.; Jackson, K. A.; Pederson, M. R.; Singh, D. J.; Fiolhais, C. Atoms, Molecules, Solids, and Surfaces: Applications of the Generalized Gradient Approximation for Exchange and Correlation. *Phys. Rev. B* **1992**, *46* (11), 6671−6687.

(29) White, J. A.; Bird, D. M. Implementation of Gradient-Corrected Exchange-Correlation Potentials in Car-Parrinello Total-Energy Calculations. *Phys. Rev. B* **1994**, *50* (7), 4954−4957.

(30) Monkhorst, H. J.; Pack, J. D. Special points for Brillouin-zone integrations. *Phys. Rev. B* **1976**, *13* (12), 5188−5192.

(31) *CRC Handbook of Chemistry and Physics*, 76th ed.; CRC Press: New York, 1996.

(32) Neugebauer, J.; Scheffler, M. Adsorbate−substrate and adsorbate−adsorbate interactions of Na and K adlayers on Al(111). *Phys. Rev. B* **1992**, *46* (24), 16067−16080.

(33) Rempel, J. Y.; Trout, B. L.; Bawendi, M. G.; Jensen, K. F. Properties of the CdSe(0001), (000$\bar{1}$), and (11$\bar{2}$0) single-crystal surfaces: relaxation, reconstruction, and adatom and admolecule adsorption. *J. Phys. Chem. B* **2005**, *109* (41), 19320−19328.